Nonlocal-density-functional approximation for exchange and correlation in semiconductors

Mark S. Hybertsen and Steven G. Louie
Department of Physics, University of California, Berkeley, California 94720
and Lawrence Berkeley Laboratory, Berkeley, California 94720
(Received 26 June 1984)

Using the weighted density approximation for the exchange-correlation energy, the band-structure and bulk structural properties of the prototypical semiconductors Si and Ge have been systematically studied. The weighted density approximation is based on an improved description of the exchange-correlation hole that explicitly accounts for the inhomogeneous charge density found in real materials. We find that the approximation as proposed is inadequate for the case of semiconductors where charge inhomogeneity is intimately connected to a gap in the excitation spectrum with consequent qualitative changes in screening. We use a simple extension of the weighted density approximation which takes account of semiconductor screening. With this functional, we find substantial improvement in the calculated minimum gap over the results of the usual local-density approximation as compared to experiment. However, the direct gaps are not significantly improved. Calculated structural properties are, moreover, found to be in excellent agreement with experiment. By way of contrast, the weighted density approximation implemented with metallic screening gives a smaller change in the band structure and more importantly, substantially poorer calculated structural properties. A discussion of the qualitative differences between the weighted density approximation and the usual local-density approximation for covalently bonded semiconductors is presented.

I. INTRODUCTION

One major difficulty in *ab initio* calculations of the properties of electronic systems is adequate treatment of the electron-electron interaction. The most commonly used approach is that of the density-functional formalism.[1] Hohenberg and Kohn established that the total energy of a system of interacting electrons in an external potential is a functional of the electron density. Furthermore, the total energy is minimized for the correct ground-state density. This is usually written in the form

$$E[n]=T_0[n]+\int d\vec{r}\, n(\vec{r})v_{\rm ext}(\vec{r})+E_H[n]+E_{\rm xc}[n]\ . \quad (1)$$

The first term is the kinetic energy of noninteracting electrons of the same density, the second term gives the energy of interaction with the external potential, the third term is the electrostatic or Hartree energy, and the last term contains the rest, the exchange-correlation (XC) energy. Given the energy functional, the problem of finding the ground-state energy is reduced to solving a set of effective one-electron equations with a local potential, the Kohn-Sham equations[2] (we use Rydberg units throughout):

$$[-\nabla^2+V_{\rm ext}(\vec{r})+V_H(\vec{r})+V_{\rm xc}(\vec{r})]\psi_i=\epsilon_i\psi_i\ . \quad (2)$$

The XC part of the effective potential is given by $V_{\rm xc}=\delta E_{\rm xc}/\delta n$, and the density n is obtained from the one-particle wave functions in the usual way.

The central difficulty is specification of $E_{\rm xc}$. The most widely used approach is the local-density approximation (LDA):[2]

$$E_{\rm xc}^{\rm LDA}=\int d\vec{r}\, n(\vec{r})\epsilon_{\rm xc}^{\rm hom}(n(\vec{r}))\ , \quad (3)$$

where $\epsilon_{\rm xc}^{\rm hom}(n)$ is the XC energy density of the homogeneous electron gas of density n. Several parametrizations of electron-gas data are in common use.[3-5] The LDA has proven very successful for calculation of ground-state properties.[6,7] Generally, the lattice constants are predicted within $\sim 1\%$ and the bulk moduli within $\sim 10\%$ of experiment. The cohesive energy is quite generally overestimated, a result usually attributed to the predicted underbinding of atoms within the LDA. On the other hand, when the ϵ_i from the Kohn-Sham equations are interpreted as quasiparticle energies, agreement with experiment is far less satisfactory. The relative positions of valence-band energies for bulk materials agree well with photoemission experiments. However, the Kohn-Sham gap given by the difference in eigenvalues for the valence-band maximum and conduction-band minimum ($\epsilon_g=\epsilon_{\rm CBM}-\epsilon_{\rm VBM}$) does not agree with the minimum gap E_g for semiconductors and insulators, although the topology of the conduction bands agree well. The minimum gaps for semiconductors and insulators are usually underestimated by 30–50 %.[7-9]

There are several distinct approaches to this problem. First, the quasiparticle energies should be obtained from the one-particle Green's function. There have been several recent approaches to this, including the work of Strinati, Mattausch, and Hanke,[10] and Wang and Pickett.[11] Hanke and co-workers have developed a tight-binding approach which includes both local-field effects and electron-hole interactions in the dynamically screened Coulomb interaction which enters the calculation of the Dyson self-energy operator. Their results for the diamond band gaps and bandwidth agree well with experiment. The approach of Wang and Pickett employed a simplified density-functional scheme with a LDA for the Dyson self-energy

operator.[12] To calculate the self-energy operator, they use the GW approximation of Hedin[13] with the screened interaction given by the model dielectric function of Levine and Louie[14] that reproduces the screening characteristic of a semiconductor. For the case of Si, they find a predominantly energy-dependent correction to the eigenvalues that greatly improves the direct gaps. Agreement with experiment for E_g is also improved.

Levine and Louie[14] recognized that because the screening of the electron-electron interaction in a semiconductor is qualitatively different from the screening in a metal, the XC energy is consequently different. To include this effect, they calculated the XC energy of a model insulating homogeneous electron gas using their model dielectric function in the scheme of Singwi *et al.*[15] The resulting LDA gave systematic (but small) improvement for the gaps in Si.

Perdew *et al.*[16] observed that, in the LDA, a single electron has a spurious interaction with itself. For a density corresponding to one electron (one orbital), n_i,

$$\delta_i = E_H[n_i] + E_{\rm xc}[n_i] \tag{4}$$

should be identically zero. Within the LDA this is not true. Perdew *et al.* have developed a self-interaction-correction (SIC) approximation wherein the spurious self-interaction δ_i is subtracted from $E[n]$ for each occupied orbital. This orbital-dependent functional gives ϵ_i values for atoms that are in much better agreement with experimental removal energies. However, for bulk materials, the correction depends on the basis used to calculate δ_i, e.g., extended versus localized basis, vanishing in the limit of large volume for the former. Heaton *et al.*[17] have done calculations for LiCl where the SIC is evaluated with a localized basis. The resulting band gap agrees much better with experiment than the LDA result. Perdew and Norman[18] have proposed a scale-independent approximation to the SIC which is essentially an energy-dependent potential. It appears to give good results for the E_g of wide-gap insulators.

Sham and Schlüter[19] (and independently, Perdew and Levy[20]) have investigated formally whether, in fact, the Kohn-Sham gap can give the true minimum gap in a semiconductor or insulator. Sham and Schlüter have shown formally that there should be a correction to the Kohn-Sham gap,

$$E_g = \epsilon_g + \Delta \ , \tag{5}$$

where Δ is the discontinuity in the functional derivative of the XC functional for a system with a gap. Their prescription for calculating Δ via many-body perturbation theory has yet to be implemented for real materials. Their results for a simple model indicate that Δ is of the same order of magnitude as ϵ_g, but whether this will still be true for real materials is unclear. Alternatively, it is not clear whether the discrepancy between E_g and the Kohn-Sham gap ϵ_g for the LDA noted above is due largely to inadequacies in the LDA. This must be addressed by doing calculations for bulk materials with improved XC functionals.

The LDA is formally valid in the limit of slowly varying electron density. However, in a semiconductor the charge is localized in bonds. Several approaches have been proposed for overcoming this problem, including gradient corrections[2,21] and the weighted density approximation (WDA).[22,23] The WDA is based on an improved description of the XC hole. Unlike the LDA, the XC-hole charge is not constrained to be spherically symmetric or centered on the electron. This clearly gives a physically more sensible description in the asymptotic regions far from an isolated atom or from a surface. As we will see in detail, this is also important for semiconductors where charge is accumulated in bonds. With the exception of the calculations of Manghi *et al.*[24] for the energy bands of GaAs, there have been no complete calculations with the WDA. In particular, no studies of structural properties have been done.

In this paper we discuss implementation of the WDA proposed by Gunnarsson *et al.*[23] As we will discuss in detail, this explicitly takes account of the inhomogeneity of the charge density as it affects the shape of the XC hole. In addition, inhomogeneity leads to a gap in the excitation spectrum for semiconductors and insulators with a corresponding change in the screening of the Coulomb interaction. This also affects the size or extent of the XC hole. One would expect that these physical effects should be treated together. The latter can be included by making use of the Levine-Louie (LL) model calculation for an insulating electron gas discussed above. In order to sort out these two effects to the degree possible, we have done two different WDA calculations: one implemented with metallic screening from the usual electron gas and the other implemented with semiconductor screening using the LL model. We have done fully-self-consistent calculations for the prototypical semiconductors Si and Ge. Our results indicate that both aspects of the inhomogeneous density of a semiconductor should be treated together. For the case where the semiconductor screening is included, we find substantial improvement for the minimum gap. In addition, in contrast to the results for the WDA with metallic screening, the structural properties for Si and Ge calculated with that functional are in excellent agreement with experiment. For the case of metallic screening, we obtain a cohesive energy which is substantially too small in contrast to the LDA. A brief report of this work has been given elsewhere.[25]

The remainder of the paper is organized as follows. In Sec. II we discuss the WDA and the resulting functional which incorporates the Levine-Louie scheme. In Sec. III the implementation of this functional for bulk calculations is described in detail. We show our results for the band structure and structural properties of Si and Ge in Sec. IV. In Sec. V we present some discussion and conclusions.

II. THE WEIGHTED DENSITY APPROXIMATION AND SEMICONDUCTOR SCREENING

We start with the following picture of the XC energy of an interacting electron system. The exchange and dynamical Coulomb interactions between electrons lead to a local

depletion of electrons around a given electron, the XC hole. The XC energy can be written exactly in terms of the charge associated with the XC hole:[23]

$$E_{\rm xc}[n]=\int\int d\vec{r}\,d\vec{r}\,' n(\vec{r})\frac{n_{\rm xc}(\vec{r},\vec{r}\,')}{|\vec{r}-\vec{r}\,'|} . \tag{6}$$

The XC hole is related to the conditional pair-correlation function $g_{[n]}$:

$$n_{\rm xc}(\vec{r},\vec{r}\,')=n(\vec{r}\,')\int_0^1 d\alpha[g_{[n]}(\vec{r},\vec{r}\,';\alpha)-1]$$
$$\equiv n(\vec{r}\,')G_n(\vec{r},\vec{r}\,') . \tag{7}$$

The pair-correlation function is evaluated for the physical density. The necessity of a coupling-constant integral can be traced to the use of T_0 in Eq. (1). Charge conservation requires that the XC hole must contain precisely one electron:

$$-1=\int d\vec{r}\,' n_{\rm xc}(\vec{r},\vec{r}\,') . \tag{8}$$

Although these relations are exact, it is generally not possible to calculate $g_{[n]}$ for an inhomogeneous system. A reasonable approximation is required.

Within the LDA, the exact functional G of the density is replaced by the corresponding homogeneous-electron-gas result evaluated for the local density, and the argument of the density prefactor is changed to the local point $\vec{r}$:

$$n_{\rm xc}^{\rm LDA}(\vec{r},\vec{r}\,')=n(\vec{r})G^{\rm hom}(|\vec{r}-\vec{r}\,'|;n(\vec{r})) . \tag{9}$$

The $\vec{r}\,'$ integration in Eq. (6) can be done straightforwardly, leading to the usual form of the XC functional in the LDA shown in Eq. (3). The XC-hole sum rule, Eq (8), is satisfied by the LDA. It is evident that the LDA XC hole is spherically symmetric and centered on the electron by construction. The usual explanation for the success of the LDA for ground-state properties despite these limitations is that $E_{\rm xc}$ depends only on the spherical average of the XC-hole charge. Satisfaction of the XC-hole sum rule leads to systematic cancellation of errors.[26]

In the WDA,[23] a better description of the XC-hole charge is attempted. The proper density prefactor is retained and G is evaluated for a density averaged essentially over the size of the XC hole:

$$n_{\rm xc}^{\rm WDA}(\vec{r},\vec{r}\,')=n(\vec{r}\,')G^{\rm hom}(|\vec{r}-\vec{r}\,'|;\bar{n}(\vec{r})) . \tag{10}$$

The parameter $\bar{n}$ is determined at each point by requiring the XC sum rule (8) be satisfied:

$$-1=\int d\vec{r}\,' n(\vec{r}\,')G^{\rm hom}(|\vec{r}-\vec{r}\,'|;\bar{n}(\vec{r})) . \tag{11}$$

The XC hole needs no longer to remain centered on the electron, and depends nonlocally on the charge density. This represents a more physically correct description of the XC hole in many situations. This approximation is exact in the homogeneous limit. It is also exact in the limit of a one-electron system, e.g., the hydrogen atom. The latter follows because the integral of $n(\vec{r})$ must be unity for this case leading to $G=-1$ as the consistent solution of Eq. (11) (i.e., $\bar{n}=0$ identically). In the sense of Zunger and Perdew,[16] the formalism is self-interaction-free: δ_i in Eq. (4) is zero.

Simple formulations of $G^{\rm hom}$ are not available. Therefore we use the analytic ansatz proposed by Gunnarsson and Jones:[27]

$$G(x;\bar{n})=C(\bar{n})(1-\exp\{-[\lambda(\bar{n})/x]^5\}) . \tag{12}$$

The parameters $C(\bar{n})$ and $\lambda(\bar{n})$ are determined by demanding that G in Eq. (12) reproduce the homogeneous limit. In particular, we require that the sum rule (8) be satisfied in that limit and that the energy density be given properly:

$$-1=\bar{n}\int d\vec{r}\,' G(|\vec{r}-\vec{r}\,'|;\bar{n}) , \tag{13a}$$

$$\epsilon_{\rm xc}^{\rm hom}(\bar{n})=\bar{n}\int d\vec{r}\,'\frac{G(|\vec{r}-\vec{r}\,'|;\bar{n})}{|\vec{r}-\vec{r}\,'|} . \tag{13b}$$

With the ansatz (12), these yield

$$\lambda(\bar{n})=-I_1/[I_2\epsilon_{\rm xc}^{\rm hom}(\bar{n})] , \tag{14a}$$

$$C(\bar{n})=-1/[I_2\bar{n}\lambda^3(\bar{n})] , \tag{14b}$$

where the constants I_1 and I_2 are given by

$$I_1=4\pi F_1(0)=4\pi\int_0^\infty y\,dy(1-e^{-1/y^5}) , \tag{15a}$$

$$I_2=4\pi F_2(0)=4\pi\int_0^\infty y^2 dy(1-e^{-1/y^5}) . \tag{15b}$$

The functions F_1 and F_2 are defined below. These integrals can easily be evaluated in terms of Γ functions. One should note that although G is specified in terms of the energy density of a homogeneous electron gas, we are really constructing the ansatz (12) such that it has the same $1/r$ moment as $G^{\rm hom}$. The XC-hole sum rule requires that they have the same zero moment.

Because we replace the exact $G^{\rm hom}$ with this simple analytic form, the one-electron system is no longer exact. The reason for this is illustrated in Fig. 1, where $C(\bar{n})$ versus $\lambda(\bar{n})$ is shown for the case of the Ceperley and Alder (CA) form of $\epsilon_{\rm xc}^{\rm hom}$.[5] Because $\lim_{\lambda\to\infty}|C|>1$, there will be a consistent nonzero $\bar{n}$ in Eq. (11), even for the case of a one-electron system. The XC-hole charge is no longer just $-n(\vec{r})$ as it must be for a one-electron system. This result is not an artifact of the particular form chosen for $G^{\rm hom}$, but rather due to its scale invariance. Only the

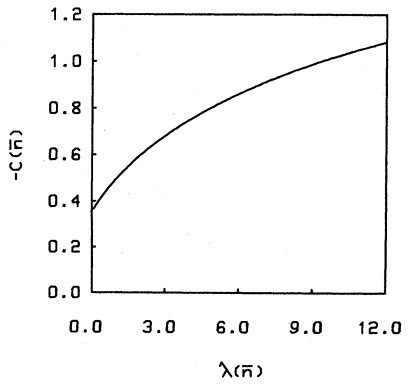

FIG. 1. Plot of the parameters $C(\bar{n})$ vs $\lambda(\bar{n})$ that determine the function $G(x;\bar{n})$ in Eq. (12). For this plot, the Ceperley-Alder XC data for the electron gas was used.

length scale (λ) and overall scale (C) depend on the density, not the shape. This is too simple to represent the detailed structure of G, even for the homogeneous electron gas. The degree of residual self-interaction in this approximation cannot be evaluated *a priori*. However, Fig. 1 suggests that for any orbital with characteristic extent less than about 4 a.u., it will be small. We have done self-consistent calculations for the hydrogen atom. The WDA with the ansatz (12) gives the total energy differing from the exact result by less than 0.1% as compared to $\sim 10\%$ within the LDA. This confirms that there is essentially no self-interaction for an electron localized on the scale of an atom for this model.

The screening built into the usual LDA is intrinsically metallic. However, screening in a semiconductor is qualitatively different due to the gap in the excitation spectrum. In the method of Singwi *et al.*[15] for treating the XC energy of the homogeneous electron gas, the spectrum enters through the irreducible polarizability, e.g., the Lindhard result, which has a metallic spectrum. Levine and Louie[14] proposed a model dielectric function appropriate for semiconductors:

$$\epsilon_2^{\mathrm{LL}}(q,\omega)=\begin{cases}\epsilon_2^{L}(q,\omega_-), & |\omega| \geq \gamma\omega_F \\ 0, & |\omega| < \gamma\omega_F\end{cases} \tag{16}$$

where ϵ^L is the Lindhard dielectric function, ω_F is the Fermi energy, and $\omega_-^2=\omega^2-(\gamma\omega_F)^2$. ϵ_1^{LL} is obtained from the Kramers-Kronig relations. The additional parameter $\gamma=\bar{E}_g/\omega_F$ is a dimensionless measure of the average gap in the optical spectrum. As such it gives a measure of the effect of the gap on screening. As discussed by Callaway,[28] this is an appropriate parameter for a perturbation expansion of the effects of the gap in a nearly-free-electron model. There, it is essentially the ratio of the gap to the bandwidth. Here the parameter γ is determined by requiring $\epsilon^{\mathrm{LL}}(q=0,\omega=0)$ reproduce the known dielectric constant. $\gamma=0.4$ is appropriate for Si and $\gamma=0.35$ for Ge. As discussed in Ref. 14, ϵ^{LL} reproduces well the numerically calculated semiconductor dielectric function for Si. It satisfies the important dielectric function sum rules.

Using this for the polarizability, Levine and Louie obtain a two-parameter- (r_s,γ) model XC energy density and chemical potential for an insulating homogeneous electron gas via the method of Singwi *et al.* In this approach, the details of the model are subsumed in the dielectric function. Alternatively, one could start with a model spectrum for a homogeneous electron gas with a gap (such as the Callaway model) and proceed directly to calculation of ϵ_{xc}. However, the advantage of the LL approach is the use of an analytically tractable dielectric function which satisfies the f-sum rules. Then one has all the information required to obtain XC data using the method of Singwi *et al.* for a model with the effect of the qualitatively different screening in a semiconductor. Physically, the effect of including a gap in the spectrum is to tighten the XC hole by folding in contributions with wave vector larger than k_F. This is illustrated in Fig. 2. The pair-correlation function computed using the usual metallic spectrum is compared to the pair-correlation function for a spectrum with a gap appropriate for Si. The quantity plotted is actually

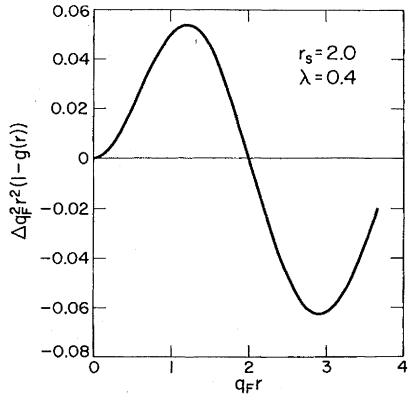

FIG. 2. Difference between the $q_F^2 r^2[1-g(r)]$ with and without the presence of a gap ($\gamma=0.4$ vs $\gamma=0.0$) for $r_s=2.0$ appropriate for Si.

$$q_F^2 r^2\{[1-g(r,\gamma=0.4)]-[1-g(r,\gamma=0)]\}$$

for $r_s=2.0$. The XC hole thus is given more weight in the region of small r at the expense of the region farther out (the XC sum rule must be satisfied).

In the formulation of the WDA with the ansatz given by Eq. (12) for G^{hom}, the nature of the screening is built in through the homogeneous limit in Eqs. (13) for determining the parameters $C(\bar{n})$ and $\lambda(\bar{n})$. Metallic screening is implicit if we demand that the WDA reduce to the usual homogeneous electron gas, e.g., the Ceperley-Alder[5] data. The effect of semiconductor screening on the size of the XC hole is accounted for by constraining the ansatz to reproduce the results of the LL model. This is done in Eqs. (14) by using the ϵ_{xc} from the LL model. We have used the interpolation formulation provided in Ref. 14 for μ_{xc}, integrating to obtain ϵ_{xc}.

At this point we would like to note that we have not given a formal derivation of this approach to including the effects of semiconductor screening. We do feel that this is a physically plausible approach. Although we refer above to a "model insulating electron gas," one should really think in terms of a description of a semiconductor where off-diagonal elements of the polarizability have been neglected. In the Levine-Louie approach the diagonal part of the dielectric matrix is calculated for a model semiconductor with the approach of Singwi *et al.* used to include the exchange-correlation effects. Then a pair-correlation function more appropriate for a semiconductor is obtained from the diagonal components. We feel that justification for this procedure is to be found *a posteriori* in the present situation, where we seek a consistent, computationally viable approximation for the XC functional in a semiconductor.

In the WDA the calculation of the XC energy is

equivalent to obtaining the XC energy density at each point. From Eqs. (6) and (7), this is given by

$$\epsilon_{xc}(\vec{r})=\int d\vec{r}\,' n(\vec{r}\,')\frac{G(|\vec{r}-\vec{r}\,'|;\bar{n}(\vec{r}))}{|\vec{r}-\vec{r}\,'|}\ , \tag{17}$$

where the ansatz (12) is used for G. In order to obtain the density, total energy, and Kohn-Sham spectrum, we need the XC potential V_{xc}. Calculation of the functional derivative from (6) gives three contributions, $V_{xc}=V_1+V_2+V_3$. These are given by

$$V_1(\vec{r})=\epsilon_{xc}(\vec{r})\ , \tag{18a}$$

$$V_2(\vec{r})=\int d\vec{r}\,' n(\vec{r}\,')\frac{G(|\vec{r}-\vec{r}\,'|;\bar{n}(\vec{r}\,'))}{|\vec{r}-\vec{r}\,'|}\ , \tag{18b}$$

$$V_3(\vec{r})=\int\int d\vec{r}\,' d\vec{r}\,''\frac{n(\vec{r}\,')n(\vec{r}\,'')}{|\vec{r}\,'-\vec{r}\,''|}\frac{\partial G(|\vec{r}\,'-\vec{r}\,''|;\bar{n})}{\partial\bar{n}}\bigg|_{\bar{n}=\bar{n}(\vec{r}\,')}\frac{\delta\bar{n}(\vec{r}\,')}{\delta n(\vec{r})}\ . \tag{18c}$$

The functional derivative of the average density $\bar{n}(\vec{r})$ can be obtained from the sum rule (11):

$$\frac{\delta\bar{n}(\vec{r}\,')}{\delta n(\vec{r})}=-G(|\vec{r}-\vec{r}\,'|;\bar{n}(\vec{r}\,'))\Big/\left[\int d\vec{r}\,''' n(\vec{r}\,''')\frac{\partial G(|\vec{r}\,'-\vec{r}\,'''|;\bar{n})}{\partial\bar{n}}\bigg|_{\bar{n}=\bar{n}(\vec{r}\,')}\right]\ . \tag{19}$$

The first term is just the energy density, while the other two terms come from the variation of the XC hole with density. In the limit of homogeneous density, the first two terms reduce to $\epsilon_{xc}^{hom}(n)$, while the third term reduces to $\mu_{xc}^{hom}(n)-2\epsilon_{xc}^{hom}(n)$. In the limit of large distance from a localized charge distribution, such as an atom, the energy density varies asymptotically as $-1/r$ (Ry units), which is the correct semiclassical behavior. The other two terms in the potential drop off faster in the large-r limit so that we also have $\lim_{r\to\infty} V_{xc}\sim -1/r$. The correct semiclassical limit would be $-2/r$. Note, in distinction, that the LDA gives an exponential dropoff at large r. For illustrative purposes, the three terms in V_{xc} are displayed in Fig. 3 for the case of the Si pseudoatom (solid lines). These are calculated for a self-consistent charge density within the WDA with the CA correlation used in the homogeneous limit. For comparison, the corresponding LDA terms are shown for the same charge density (dashed lines). We also remark that Gunnarsson and Jones chose the ansatz in Eq. (12) to reproduce within the WDA the proper image behavior of an electron far from a metal surface.

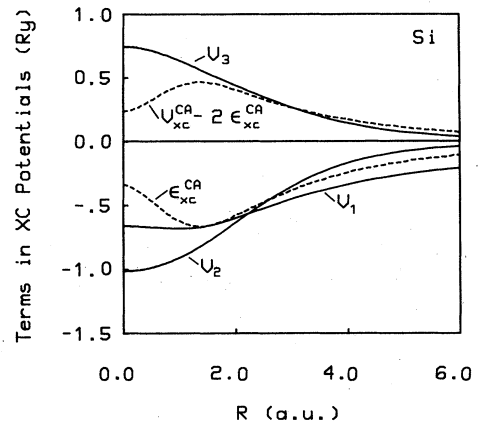

FIG. 3. Comparison of the three terms in the WDA XC potential to the corresponding LDA terms for the case of the Si pseudoatom. V_1, V_2, and V_3 are calculated from the charge density of the pseudoatom done self-consistently within the WDA (CA XC data used to obtain the parameters C and λ). The terms from the LDA cases are calculated for the same charge density and are for the CA XC data.

The previous WDA calculation of the Si band structure by Kerker[29] was done with a drastic approximation for V_{xc}. He assumed that $V_2\equiv V_1$ and that $V_3\equiv 0$. With this approximation, the homogeneous limit of V_{xc} is incorrect. In fact, from that limit we see that his approximation is analogous to $\alpha=1$ in the $X\alpha$ approximation, as pointed out by Wang and Pickett.[11] In the calculations for Rh of Borstel *et al.*,[30] similar approximations were employed. For calculations on Cu, Przybylski and Borstel[31] continue to force $V_2\equiv V_1$, but include V_3 with a local-type approximation. Here we correctly incorporate all the terms of V_{xc} in the calculation without simplifying approximation.

III. DETAILS OF THE CALCULATION

A. Calculation of the exchange-correlation energy and potential

We restrict the discussion to the case of crystalline solids (or, more generally, systems with periodicity). For other cases, such as atoms with spherical symmetry, other numerical approaches to calculating the XC energy and potential may be more appropriate. We will take up the case of atoms in particular in a future publication.

For the periodic case, we expand the charge density in a Fourier series in reciprocal space:

$$n(\vec{r})=\sum_{G} n(\vec{G})e^{i\vec{G}\cdot\vec{r}}\ . \tag{20}$$

Then, to obtain the XC energy, we need to calculate the XC energy density at each point in the real-space cell. Kerker has discussed this calculation.[29] Using (20) in expression (17) for ϵ_{xc} yields

$$\epsilon_{xc}(\vec{r})=4\pi C(\vec{r})\lambda^2(\vec{r})\sum_{\vec{G}} n(\vec{G})e^{i\vec{G}\cdot\vec{r}}F_1(q)\Big|_{q=\lambda(\vec{r})G} \tag{21}$$

A compressed notation for C and λ has been adopted, in which it is understood that the spatial dependence of these parameters comes from their dependence on $\bar{n}(\vec{r})$. The function $F_1(q)$ is defined by

$$F_1(q)=\frac{1}{q}\int_0^\infty dy(1-e^{-1/y^5})\sin(qy)\ . \tag{22}$$

The average density $\bar{n}(\vec{r})$ is determined at each point by the requirement that the sum rule (11) be satisfied. Using (20) yields, for the sum rule,

$$-1=4\pi C(\vec{r})\lambda^3(\vec{r})\sum_{\vec{G}} n(\vec{G})e^{i\vec{G}\cdot\vec{r}}F_2(q)\Big|_{q=\lambda(\vec{r})G}\ . \tag{23}$$

In our calculation we start with an initial value for $\bar{n}$ and augment it iteratively until (23) is satisfied to 1 part in 10^{-6}. The function $F_2(q)$ is defined by

$$F_2(q)=\frac{1}{q}\int_0^\infty y\,dy(1-e^{-1/y^5})\sin(qy)\ . \tag{24}$$

The functions F_1 and F_2 are calculated once on a uniform grid and stored. Required values are obtained by interpolation.

In the calculation of the potential V_{xc}, the first term is given by (21) above. For the second and third terms, an alternative approach is required. If the Fourier components of V_2 are examined directly and use is made of (20), the result is

$$V_2(\vec{G})=\frac{4\pi}{\Omega}\int d\vec{r}\,'n(\vec{r}\,')C(\vec{r}\,')e^{-i\vec{G}\cdot\vec{r}\,'}F_1(q)\Big|_{q=\lambda(\vec{r}\,')G}\ , \tag{25}$$

where Ω is the volume of the unit cell. The third term is somewhat more involved. Note first that, upon rearrangement, one has

$$V_3(\vec{r})=-\int d\vec{r}\,'n(\vec{r}\,')\frac{h_1(\vec{r}\,')}{h_2(\vec{r}\,')}G(|\vec{r}-\vec{r}\,'|;\bar{n}(\vec{r}\,'))\ , \tag{26}$$

where the functions h_1 and h_2 are defined by

$$h_1(\vec{r}\,')=\int d\vec{r}\,''\frac{n(\vec{r}\,'')}{|\vec{r}\,'-\vec{r}\,''|}\frac{\partial G(|\vec{r}\,'-\vec{r}\,''|;\bar{n})}{\partial\bar{n}}\Big|_{\bar{n}=\bar{n}(\vec{r}\,')}\ , \tag{27a}$$

$$h_2(\vec{r}\,')=\int d\vec{r}\,'''n(\vec{r}\,''')\frac{\partial G(|\vec{r}\,'-\vec{r}\,'''|;\bar{n})}{\partial\bar{n}}\Big|_{\bar{n}=\bar{n}(\vec{r}\,')}\ . \tag{27b}$$

Then, V_3 can be calculated in the same way as V_2:

$$V_3(\vec{G})=-\frac{2\pi}{\Omega}\int d\vec{r}\,'n(\vec{r}\,')\frac{h_1(\vec{r}\,')}{h_2(\vec{r}\,')}C(\vec{r}\,')\lambda^3(\vec{r}\,')\times e^{-i\vec{G}\cdot\vec{r}\,'}F_2(q)\Big|_{q=\lambda(\vec{r}\,')G}\ . \tag{28}$$

Calculation of V_3 is reduced to obtaining the auxiliary functions $h_1(\vec{r})$ and $h_2(\vec{r})$. Note that with the ansatz (12), the required derivative of G is given by

$$\frac{\partial G(x;\bar{n})}{\partial\bar{n}}=\alpha(\bar{n})G(x;\bar{n})+\beta(\bar{n})e^{-(\lambda/x)^5}/x^5\ , \tag{29}$$

where the parameters α and β are

$$\alpha(\bar{n})=\frac{1}{C(\bar{n})}\frac{\partial C}{\partial\bar{n}}\ , \tag{30a}$$

$$\beta(\bar{n})=5C(\bar{n})\lambda^4(\bar{n})\frac{\partial\lambda}{\partial\bar{n}}\ . \tag{30b}$$

From the form of (29), the first terms of h_1 and h_2 are proportional to ϵ_{xc} and the sum rule, respectively. The second terms can be computed in an analogous fashion as they are of convolution form. The result is

$$h_1(\vec{r})=2\alpha(\vec{r})V_1(\vec{r})+\frac{8\pi\beta(\vec{r})}{\lambda^3(\vec{r})}\sum_{\vec{G}} n(\vec{G})e^{i\vec{G}\cdot\vec{r}}F_3(q)\Big|_{q=\lambda(\vec{r})G}\ , \tag{31a}$$

$$h_2(\vec{r})=-\alpha(\vec{r})+\frac{4\pi\beta(\vec{r})}{\lambda^2(\vec{r})}\sum_{\vec{G}} n(\vec{G})e^{i\vec{G}\cdot\vec{r}}F_4(q)\Big|_{q=\lambda(\vec{r})G}\ . \tag{31b}$$

Compressed notation is used for α and β as before. The auxiliary functions $F_3(q)$ and $F_4(q)$ are defined by

$$F_3(q)=\frac{1}{q}\int_0^\infty\frac{dy}{y^5}e^{-1/y^5}\sin(qy)\ , \tag{32a}$$

$$F_4(q)=\frac{1}{q}\int_0^\infty\frac{dy}{y^4}e^{-1/y^5}\sin(qy)\ . \tag{32b}$$

As for F_1 and F_2, these are computed once for a uniform grid, and needed values are obtained by interpolation.

Since we use a pseudopotential formalism, the charge density is smooth and can be obtained in real space by fast Fourier transform from reciprocal space. Functions defined on the uniform grid in real space then contain equivalent information to those in reciprocal space. Required real-space integrations are replaced by summations. Since ϵ_{xc}, C, λ, etc. are required for all points in the real-space cell, the crystal symmetry is used to effectively confine the need to calculate these to the irreducible wedge of the real-space cell. We have found that the added cost of calculating V_{xc} within this WDA is marginal compared to the cost of matrix diagonalization for the case of the diamond structure.

TABLE I. Comparison of pseudoatom calculations where the ionic pseudopotential is screened with the WDA to all-electron atom calculations where the screening is done with the WDA in a shell-partitioned model. Results for two configurations of Si are shown. Energies are reported in Ry.

Configuration	State	Pseudoatom	Shell partition	δ
Si s^2p^2	ϵ_s	−0.8494	−0.8371	0.0123
	ϵ_p	−0.3551	−0.3480	0.0071
Si s^1p^3	ϵ_s	−0.9023	−0.8915	0.0108
	ϵ_p	−0.3946	−0.3878	0.0068
ΔE_{total}		−0.5012	−0.4966	0.0046

B. Implementation of the pseudopotential formalism

In the present calculations, the *ab initio* ionic pseudopotential is generated from the all-electron atom by the method of Kerker.[32] For generation of the pseudopotential, the singly ionized configuration $s^2p^{0.8}d^{0.2}$ is used to obtain the s, p, and d potentials. The r_c parameter[32] entering the generation of the potentials is chosen to be $r_{c,s}=1.58$, $r_{c,p}=1.93$, and $r_{c,d}=1.93$ for Si, and $r_{c,s}=1.57$, $r_{c,p}=2.02$, and $r_{c,d}=2.38$ for Ge. We found the potentials to have excellent transferability to the ground-state and nearby excited configurations (e.g., s^1p^3) with eigenvalues reproduced to within ~ 1 mRy and total-energy differences better.

The atomic all-electron calculation is done using the LDA with the CA form. Thus, the intershell XC interaction frozen into the ionic pseudopotential is within the LDA. Then when the ionic pseudopotential is used in the bulk calculation or in a pseudoatom, it is screened with the WDA. This approximation is similar to the shell-partitioning ansatz proposed by Gunnarsson *et al.* in conjunction with their introduction of the WDA.[23] The original idea was that the WDA would adequately represent the intrashell XC effects but overestimate the intershell XC interaction. They argue that the LDA better represents intershell effects and suggest dividing the atomic charge density into the usual shells for purposes of calculating E_{xc}. The intrashell part is done within the WDA and the intershell part is calculated using the LDA.

We have quantitatively compared our use of an ionic pseudopotential generated from an atom calculated using the LDA with the shell-partitioning ansatz for the case of Si. We first do self-consistent pseudoatom calculations where the screening is done with the WDA using CA XC data in the homogeneous limit as described in Sec. II above. For comparison, we next do self-consistent all-

TABLE II. Comparison of calculated band energies at high-symmetry points to experiment for Si. The four different calculations displayed are discussed in the text. The energies are reported in eV and are referred to the valence-band maximum.

	Silicon				
	LDA		Present work		
	CA	LL	WDA(CA)	WDA(LL)	Expt.[a]
E_g	0.56	0.70	0.71	0.90	1.17
$\Gamma_{1,v}$	−11.92	−11.87	−11.85	−11.78	−12.5±0.6
$\Gamma_{25',v}$	0.00	0.00	0.00	0.00	0.0
$\Gamma_{15,c}$	2.57	2.65	2.69	2.81	3.37
$\Gamma_{2',c}$	3.29	3.33	3.27	3.34	4.2
$X_{1,v}$	−7.77	−7.74	−7.74	−7.69	
$X_{4,v}$	−2.86	−2.82	−2.80	−2.74	2.9[b]
$X_{1,x}$	0.71	0.85	0.87	1.06	1.30[c]
$L_{2',v}$	−9.58	−9.55	−9.55	−9.50	−9.3±0.4
$L_{1,v}$	−6.97	−6.90	−6.89	−6.80	−6.7±0.2
$L_{3',v}$	−1.21	−1.19	−1.18	−1.16	−1.2±0.2
$L_{1,c}$	1.55	1.63	1.62	1.73	2.1[d]
$L_{3,c}$	3.40	3.50	3.54	3.68	3.9±0.1[b]

[a]Reference 35 except where noted.
[b]Reference 36.
[c]Estimated from conduction-band minimum and longitudinal effective mass.
[d]Reference 37.

TABLE III. Comparison of calculated band energies at high-symmetry points to experiment for Ge. The four different calculations displayed are discussed in the text. Energies are reported in eV and are referred to the valence-band maximum.

	Germanium				
	LDA		Present work		
	CA	LL	WDA(CA)	WDA(LL)	Expt.[a]
E_g	0.52	0.58	0.60	0.69	0.74
$\Gamma_{1,v}$	−12.50	−12.47	−12.45	−12.40	−12.6
$\Gamma_{25',v}$	0.00	0.00	0.00	0.00	0.0
$\Gamma_{2',c}$	0.74	0.75	0.74	0.78	0.89
$\Gamma_{15,c}$	2.58	2.63	2.71	2.79	3.21
$X_{1,v}$	−8.57	−8.56	−8.55	−8.52	
$X_{4,v}$	−3.03	−3.00	−2.97	−2.92	−3.15±0.2
$x_{1,c}$	0.80	0.91	0.95	1.11	1.3 ±0.2
$L_{2',v}$	−10.38	−10.36	−10.35	−10.32	−10.6 ±0.5
$L_{1,v}$	−7.40	−7.36	−7.34	−7.28	−7.7 ±0.2
$L_{3',v}$	−1.38	−1.37	−1.35	−1.33	−1.4 ±0.3
$L_{1,c}$	0.52	0.58	0.60	0.69	0.74
$L_{3,c}$	3.74	3.82	3.88	3.99	4.3 ±0.2

[a]Reference 35.

electron atom calculations with the shell-partitioning ansatz implemented as follows. The atomic charge density is partitioned into only core and valence shells. The intrashell XC is calculated using the WDA with CA XC in the homogeneous limit. The intershell XC is treated in the LDA with the CA form. The details of these atomic calculations will be described elsewhere. Table I shows the results of these calculations for two configurations of Si. The Kohn-Sham eigenvalues for the valence electrons are shown for the pseudoatom and the shell-partitioned all-electron atom in Rydbergs. In addition, the difference in total energy for the two configurations is shown. The comparison shows small differences. In particular, the difference in total energy is well reproduced. Thus, our approach is quantitatively similar to the shell-partitioning approach.

The band structure and total energy are calculated with the usual pseudopotential approach.[33] We use a plane-wave basis to expand the Hamiltonian. For the calculation of the band structure, plane waves with kinetic energy up to 14 Ry are included in the basis, and the calculation is done for the experimental lattice constant. This assures convergence of the eigenvalues to within better than 0.05 eV in general, and about 0.1 eV for the $\Gamma_{2',c}$ state in Si, which converges more slowly. For the calculation of structural properties, a cutoff of 11.5 Ry was used. Ten special $\vec{k}$ points[34] in the irreducible Brillouin zone are used for computing the charge density and other quantities requiring a sum over the Brillouin zone.

IV. RESULTS FOR SILICON AND GERMANIUM

A. Band structure

Our results for the band energies of Si and Ge at high-symmetry points are displayed in Tables II and III, respectively. Results of four different calculations are compared to experimental values largely obtained from optical and photoemission experiments.[35–37] The first two columns show the results of LDA calculations with CA and LL correlation for reference. These results agree well with previous calculations.[7,14] The second two columns show our WDA calculations. We have done calculations with both the case of CA correlation in the homogeneous limit and the LL XC data in the homogeneous limit. This allows some evaluation of the relative contributions from nonlocality and semiconductor screening (LL scheme) as discussed in Sec. II.

The minimum gap is indirect in both Si and Ge. For Si the conduction-band minimum is evaluated at 85% of the distance to the zone edge along Δ. In Ge it is at the symmetry point L. For both Si and Ge the discrepancy with experiment for E_g is significantly reduced when both nonlocality (WDA) and the gap in the spectrum (LL) are accounted for in the XC. (Note that relativistic effects, including spin-orbit couplings, are neglected in this calculation, and would reduce the calculated minimum gap in Ge.) The effects of nonlocality and semiconductor screening are comparable in magnitude for the minimum gap.[38] A similar effect is seen for the conduction-band energies at X and L which are consistently improved. However, the direct gaps are not substantially improved. In particular, the $\Gamma_{2',c}$ state in Si is very insensitive to these changes in the XC potential. For the valence-band states, the dispersion in the upper valence band is somewhat weaker than that in the LDA. The bandwidths are consistently narrowed.

To obtain some insight into these changes, we examine the XC potentials. Contour plots of the XC potential in the $(1\bar{1}0)$ plane of Si for the four cases considered here are given in Fig. 4. In each case the self-consistent potential

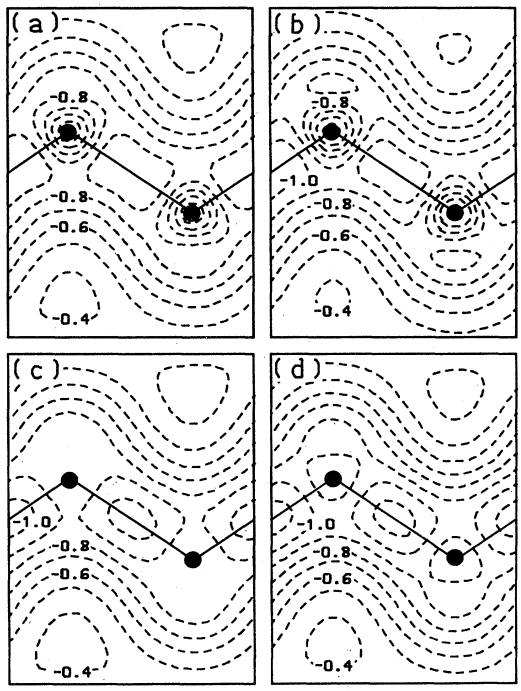

FIG. 4. Contour plots in the $(1\bar{1}0)$ plane of the self-consistent XC potential for the four different calculations reported in the text of Si: (a) is the LDA with the CA XC data, (b) is the LDA with the LL XC data, (c) is the WDA(CA), and (d) is the WDA(LL). The bond chain is indicated for each case. Dashed lines denote negative contours. The contour interval is 0.1 Ry. Refer to Table IV for values of the potentials at symmetry sites.

is shown. To aid in detailed comparison, the value of the XC potentials at several symmetry sites in the unit cell are given in Table IV. The implementation of the semiconductor screening in a LDA as done by Levine and Louie [Fig. 4(b)] leads to an XC potential that is qualitatively the same as in the usual LDA [Fig. 4(a)]. However, it is deeper at every point in the unit cell because the XC hole is tighter, as discussed in Sec. II above and in Ref. 14. The improvement in the gaps and decrease in the valence-band dispersions is largely due to the relative lowering in energy of the valence-band maximum ($\Gamma_{25',v}$ complex). As can be seen from Table IV, the XC potential in the bonding region is more negative with respect to the atomic site and interstitial region than for the usual LDA.

Implementation of the WDA(CA) [Fig. 4(c)] leads to a qualitative change in the XC potential in the region near the atomic sites. The XC potential is relatively smoother going along the bond chain. The reason for this can be seen as follows. The size of the XC hole is determined by an average of the charge density over the XC hole. This is typically of order 2 a.u. for an electron in the bond chain of Si. (See the discussion of Fig. 5 below.) That this does not change much from the bond region to the atomic site is due, in the first case, to the fact that the XC hole encompasses most of a bond, whereas in the second case the XC hole samples part of each of the four tetrahedral bonds. As a result, the parameter $\bar{n}$ varies by only about 10% from the bond region to the atomic site, and the smoother potential results. Furthermore, the deepest point in the bonding region is precisely at the center of the bond, in contrast to the LDA case where the charge density, and hence the XC potential, shows a slight double-peak (-well) structure. This is attributable to the nonlocal dependence of V_{xc} on the charge.

Quantitatively, the WDA also gives an XC potential that is relatively deeper in the bond region as compared to the interstitial region. This gives the improvement in the indirect gap, as the conduction-band states near X are predominantly in the interstitial region. The null results for the direct gaps at Γ come from a more subtle interplay between the deeper XC potential on the atomic sites and the steeper rise of the potential away from the bond chain. This is particularly true for the $\Gamma_{2',c}$ state which is centered on the atomic sites but extends into the antibonding direction.

The effect of coupling the semiconductor screening to the WDA [Fig. 4(d)] is similar to the LDA case. The tighter XC hole leads to an enhancement of the deeper XC potential in the bond region relative to the interstitial region. Consequently, the indirect gap is further improved. We show a contour plot of the parameter λ in Fig. 5 for both the WDA(CA) and the WDA(LL) cases in Si. Table V gives values at symmetry sites. As noted above, the size of the XC hole in Si is of order 2 a.u. It varies very slightly along the bond chain, but by $\sim 30\%$ going into the interstitial region. In addition, as shown in Fig. 2, the semiconductor screening results in a tighter XC hole.

TABLE IV. Comparison of the XC potentials for Si at symmetry points for the four different calculation schemes discussed in the text. Potentials are reported in Ry. Refer to Fig. 4.

Site	CA	LL	WDA(CA)	WDA(LL)
Atomic	−0.411	−0.437	−0.807	−0.832
Bonding	−0.984	−1.063	−1.044	−1.142
Antibonding	−0.682	−0.727	−0.666	−0.707
Hexagonal	−0.371	−0.388	−0.361	−0.371

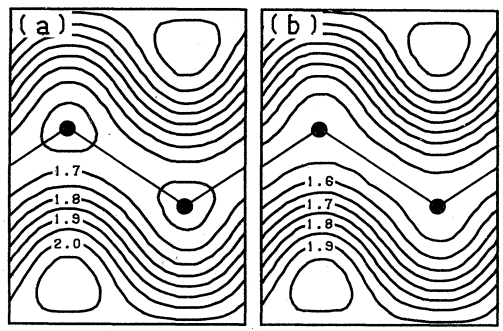

FIG. 5. Contour plots in the $(1\bar{1}0)$ plane of Si of the parameter λ that enters the ansatz Eq. (12) for $G(\vec{r})$ for the cases (a) WDA(CA) and (b) WDA(LL). Both are calculated from self-consistent charge densities. The contour interval is 0.05 a.u. Refer to Table V for values at symmetry sites.

TABLE V. Comparison of the parameter λ at symmetry sites for the two cases WDA(CA) and WDA(LL) in Si based on self-consistent charge densities in each case. λ is given in a.u. Refer to Fig. 5.

Site	λ(CA)	λ(LL)
Atomic	1.66	1.52
Bonding	1.63	1.51
Antibonding	1.84	1.73
Hexagonal	2.09	1.99

To further illustrate the structure of the WDA, we show a contour plot of each of the three terms in the XC potential in Figs. 6 and 7 for the case of the WDA(CA) in Si. Included for comparison is the corresponding LDA term in each case calculated for the same charge density. Table VI gives the values of the potentials at symmetry points. Figure 6 shows V_1 (the energy density) and V_2 for the WDA and ϵ_{xc}^{LDA}. The qualitative difference between V_1 and the LDA energy density is similar to that discussed above for the full XC potential. Quantitatively, the WDA energy density is significantly deeper on the atomic site and in the interstitial region. However, the LDA energy density is slightly deeper in the bonding region (for the same charge density), leading to only small changes in total energy between the two schemes. In general, the WDA energy density is smoother through the unit cell. The WDA V_2, which also reduces to ϵ_{xc} in the homogeneous limit, shows stronger variation through the unit cell. We can understand this with reference to Eq. (18b). The density argument of the pair-correlation function is effectively averaged over the unit cell. Viewing the function G as a cutoff function in the Coulomb integral, the parameter $\bar{n}(\vec{r}')$ determines the cutoff radius λ discussed in Sec. III A and illustrated in Fig. 5. This is smaller in the bond chain than in the interstitial region. For a point in the bond chain, the effect of the integration in Eq. (18b) is to include a λ larger, on average, than that for the case of the energy density in Eq. (17). The result is that V_2 is deeper than V_1 along the bond chain. On the other hand, for a point in the interstitial region, the situation is reversed leading to V_1 deeper than V_2. Physically, the differences between V_1 and V_2 arise from the lack of symmetry of G under interchange of $\vec{r}$ and $\vec{r}'$ in the WDA. The ramifications of this for asymptotic regimes was discussed in Sec. II above.

In Fig. 7 we show a contour plot of V_3 for the case of the WDA(CA) in Si as well as the corresponding LDA term in the XC potential. With the exception of the atomic site, the qualitative and quantitative differences are minimal. In fact, a local approximation for V_3 would probably not effect the total-energy results appreciably. However, the direct gaps at Γ would probably be worse, as the total potential would be deeper on the atomic sites.

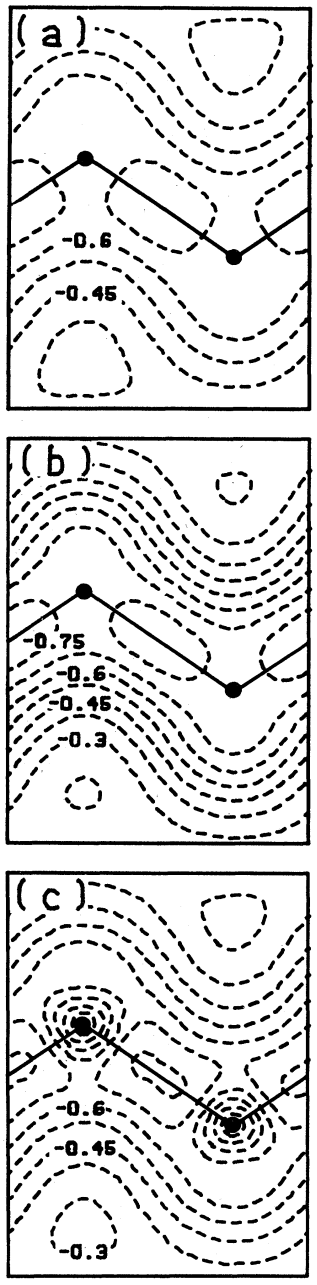

FIG. 6. Contour plots in the $(1\bar{1}0)$ plane of Si comparing (a) V_1 and (b) V_2 in the WDA XC potential to (c) the LDA energy density calculated from the same charge density (self-consistent calculation with WDA). Both cases use the CA XC data. The conventions are the same as for Fig. 4 with contour interval 0.075 Ry. Refer to Table VI for values of the potentials at symmetry sites.

B. Ground-state properties

To investigate the structural properties predicted by the WDA, we have calculated the total energy as a function of the lattice constant. We use nine different lattice constants, giving cell volumes ranging from 80% to 110% of the equilibrium value. These results are then fitted to the Murnaghan equation of state.[39] The fit obtained typically displays a rms variation of 0.1 mRy per atom or less. From the fit parameters we obtain the equilibrium lattice constant, bulk modulus, and pressure derivative of the

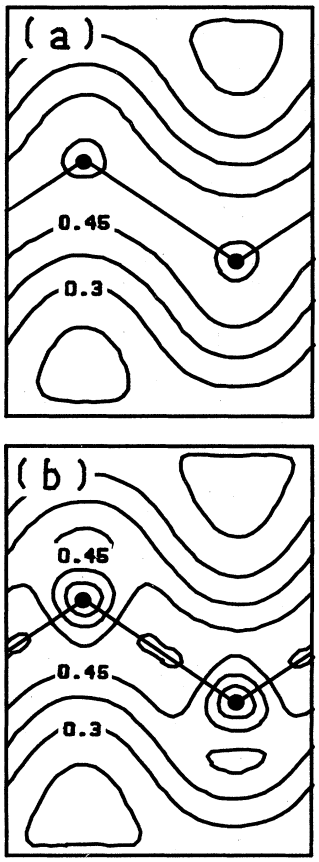

FIG. 7. Contour plots in the $(1\bar{1}0)$ plane of Si comparing (a) V_3 in the WDA XC potential to (b) the LDA $\mu_{xc}-2\epsilon_{xc}$, as in Fig. 6. The conventions are the same as for Fig. 4 with contour interval 0.075 Ry. Refer to Table VI for values of the potentials at symmetry sites.

bulk modulus at zero pressure, as well as the equilibrium energy per atom. The cohesive energy is obtained by comparing the equilibrium energy of the solid per atom extrapolated to full convergence to the total energy of the pseudoatom calculated with the same XC scheme. The correction for zero-point motion is included in the cohesive energy using a Debye model (but is neglected for the structural properties, not affecting those results within the reliability of the calculations). The total energy per atom is found to be converged to within ~ 1 mRy with a plane-wave cutoff of 20 Ry. The equilibrium energy of the solid obtained at a 11.5-Ry cutoff is corrected for convergence. The correction is taken to be the total-energy difference between 20- and 11.5-Ry cutoff calculations.

Our results, together with experimental results,[35,40,41] are displayed in Table VII. We have included calculations with the LDA using CA XC data for reference. These results agree well with previous calculations for Si and Ge within the established reliability of these types of calculations (1% for lattice constant and 10% for bulk modulus).[7] The cohesive energy is larger than in the previous calculation. This is largely attributable to the use of different XC data in the present calculation. From Table VII it is clear that the WDA(LL), which includes the semiconductor screening, gives structural properties in good agreement with experiment. The results are comparable to those obtained with the LDA. The cohesive energy requires calculation of the atomic total energy using an XC scheme consistent with the WDA(LL). The Levine-Louie model is not directly applicable to isolated atoms, so we have not been able to calculate the cohesive energy predicted by this XC functional. The solid-state results are comparable to those obtained with the LDA.

The WDA(CA), on the other hand, gives results that do not agree so well with experiment. In this case we are also able to obtain the cohesive energy. The Si and Ge atomic ground states are triplet configurations. We do the WDA(CA) calculation for the singlet configuration and take the small spin-polarization correction from LDA calculations. The result is that the crystal is underbound by $\sim 30\%$. This seems to be consistent with a lattice constant that is too large. The overestimation of cohesive energies found quite generally in LDA calculations is often attributed to underbinding in the atomic calculation (consistent with total energies found for light atoms). In the case of the WDA(CA), most of the change is due to overbinding in the pseudoatom. In Sec. IV A we discussed the energy density in the WDA(CA) as compared to the LDA. As noted, the differences largely cancel, giving a small net change in the total energy in the crystal, typically ~ 20 mRy/atom. However, examination of the corresponding pseudoatom results shown in Fig. 3 for Si reveals a different situation. The energy density for the WDA is consistently deeper than the energy density for the LDA for the same charge density. As a result, the WDA(CA) pseudoatom is ~ 0.2 Ry deeper than the LDA pseudoatom. This is consistent with our results for light atoms calculated self-consistently within WDA(CA) using the shell-partitioned ansatz of Gunnarsson *et al.* and with their first-order perturbation results.[27]

In Table VIII we show the x-ray form factors calculated with the WDA(LL) as compared to LDA results and experiment.[42–44] The valence-charge form factors are

TABLE VI. Comparison of the terms in the WDA(CA) XC potential to the corresponding LDA terms for the same charge density in Si [self-consistent calculation with WDA(CA)]. Potentials are reported in Ry. Refer to Figs. 6 and 7.

Site	V_1	V_2	ϵ_{xc}^{LDA}	V_3	$V_{xc}^{LDA}-2\epsilon_{xc}^{LDA}$
Atomic	−0.622	−0.720	−0.299	0.535	0.209
Bonding	−0.735	−0.806	−0.759	0.497	0.527
Antibonding	−0.536	−0.483	−0.520	0.353	0.363
Hexagonal	−0.346	−0.219	−0.281	0.204	0.197

TABLE VII. Comparison of the calculated equilibrium structural properties to experiment for Si and Ge.

	Lattice constant (Å)	Bulk modulus (kbar)	Cohesive energy (eV)
		Si	
LDA	5.40	940	5.28
Present work			
WDA(CA)	5.48	850	3.19
WDA(LL)	5.39	940	
Expt.	5.43[a]	990[b]	4.63[c]
		Ge	
LDA	5.60	730	4.67
Present work			
WDA(CA)	5.68	620	2.64
WDA(LL)	5.61	700	
Expt.	5.65[a]	770[b]	3.85[c]

[a]Reference 40, extrapolated to 0 K.
[b]Reference 35, measured at 77 K.
[c]Reference 41.

taken from self-consistent calculations with the experimental lattice constant and plane-wave cutoff of 14 Ry. The core charge is taken from a self-consistent LDA atomic calculation for the ground-state configuration. The LDA results agree well with previous calculation. The WDA(LL) results give only a small change. The form factors are dominated by the core charge. However, we do notice that the forbidden (222) component agrees somewhat better with experiment for the case of Si, but worse for the case of Ge.

TABLE VIII. Comparison of calculated x-ray form factors to experiment for Si and Ge. Units are electrons per unit cell. The calculations displayed are discussed in the text.

$\vec{G}$	LDA	Present work	Expt.[a]
		Silicon	
(111)	15.10	15.16	15.19
(220)	17.23	17.25	17.30
(311)	11.24	11.23	11.35
(222)	0.34	0.39	0.38
(400)	14.76	14.74	14.89
(331)	10.08	10.09	10.25
		Germanium	
(111)	38.75	38.81	39.42
(220)	47.23	47.26	47.44
(311)	31.15	31.14	31.37
(222)	0.28	0.32	0.27
(400)	40.47	40.46	40.50
(331)	27.30	27.31	27.72

[a]References 42–44.

V. DISCUSSION AND CONCLUSIONS

In the WDA(LL) approach for XC in a semiconductor, two important improvements over the usual LDA are brought together. We wish to discuss each in more detail.

Because the density prefactor in the XC hole in Eq. (10) has the proper argument, the XC hole, in general, is displaced from the electron at $\vec{r}$ and is anisotropic, reflecting the actual electron density. We have illustrated this for the case of Si in Figs. 8–10. Part (a) of each figure is a contour plot of the XC hole in the LDA. In lieu of the actual pair-correlation function for the homogeneous electron gas, we use the analytic form (12). The result reproduces the ϵ_{xc}^{LDA}, but may differ in detail from the actual XC hole in LDA. In part (b) of each figure a contour plot of the XC hole in the WDA(LL) is shown. In each case, the contour plot is for the $(1\bar{1}0)$ plane, the electron location $\vec{r}$ is shown by a plus, and appropriate bond chains are drawn. Figure 8 is for the case of an electron in the center of the bond. In the LDA the XC hole is spherically symmetric and centered on the electron, as for all locations. In the WDA the XC hole remains centered on the bond because of the symmetry of the charge density, but it has the shape of the charge density in the bond region. Figure 9 is for the case of an electron at the antibonding site. Now the XC hole in the WDA is shifted away from the electron toward the bonds: the one in the plane of the figure and the two that are in a plane perpendicular to the page. Figure 10 is for the case of an electron at the center of the fcc cubic cell. Once again, the XC hole in the WDA is shifted toward the prominent features in the charge density.

The anisotropy in the XC hole is not expected to have a large effect on the total energy. As discussed in Sec. IV B,

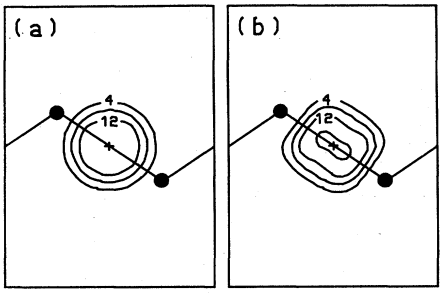

FIG. 8. Contour plots in the $(1\bar{1}0)$ plane of Si comparing the XC-hole charge for an electron at the bonding site (denoted by a +) for (a) the LDA to (b) that for the WDA(LL). The contour interval is 4.0, in units of electrons per cell.

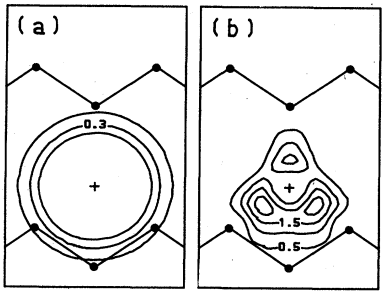

FIG. 10. Same as in Fig. 8 for an electron at the hexagonal site. The contour interval in (a) is 0.15, in units of electrons per cell. The contour interval in (b) is 0.5, in units of electrons per cell.

this is true as regards the percentage change in total energy from LDA to WDA(CA). However, as a function of volume, the results of the WDA(CA) are not so close to the LDA, thus changing the structural properties. We do expect the details of the XC hole to affect the XC potential and hence the spectrum. However, the net effect is somewhat subtle, leading to relatively small changes in most features of the band structure. In essence, the WDA introduces a different relationship between the total energy and potential (charge density). The changes in density are minor, but the smoother XC potential along the bond chain is sufficient to yield a softer bulk modulus.

The second feature we have incorporated is the effect of semiconductor screening. This enters through the size or extent of the XC hole via G^{hom} in Eq. (12). As illustrated in Figs. 2 and 5, the resulting XC hole is tighter than in the corresponding metallic case. Our results for structural properties in Si and Ge seem to reinforce one's intuitive belief that this aspect of the charge inhomogeneity must be treated together with the nonlocality of the XC hole.

We feel that our results using the WDA(CA) show that the success of the LDA cannot be completely explained by the cancellation of errors discussed in Sec. II. It seems to also be related to the consistency of the approximation. It is based on the Thomas-Fermi idea of a local electron gas, that is, an intrinsically metallic system, and so the use of the energy density of the metallic jellium model is consistent. However, in the WDA, the XC energy samples the charge density over a length of the order of a bond length. Thus it is somewhat sensitive to the very features of the charge density which we associate with the opening of a gap in the spectrum. In this way it is plausible that a consistent approximation requires inclusion of the effects of semiconductor screening. More generally, a nonlocal XC functional must interpolate properly between the screening required by the spectra of excitations from the atomic to metallic limit. This requires a more general formulation than given here.

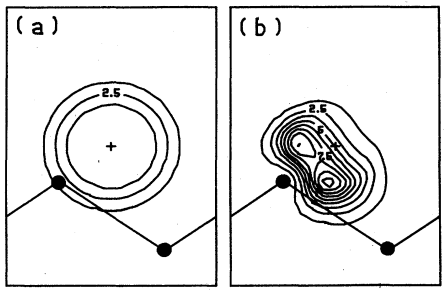

FIG. 9. Same as in Fig. 8 for an electron at the antibonding site. The contour interval is 1.25, in units of electrons per cell.

The WDA(LL) functional gives both an improved minimum gap and good structural properties. This is in contrast to the situation found in $X\alpha$ calculations for rare-gas solids. If α is chosen to fit atomic properties (e.g., the virial theorem α), calculated structural properties are reasonable, but the minimum gap is similar to the LDA result (i.e., $\sim 70\%$ of experiment). On the other hand, a larger value of α can be chosen to fix the gap, but only at the expense of poorer calculated structural properties and bandwidths.[45]

In summary, we have done band-structure and total-energy calculations for the prototypical semiconductors Si and Ge using XC functionals that go beyond the LDA. The WDA is based on an improved description of the XC hole for inhomogeneous electron systems. We find that using the usual metallic screening in the WDA yields small improvements in the band gaps, but predicts structural properties in worse agreement with experiment than the LDA results. This approximation also substantially underestimates the cohesive energy, largely due to overbinding in the atom. We have found that a consistent and effective way of implementing the WDA is with semiconductor screening. The resulting, calculated Kohn-Sham minimum gap is in significantly better agreement with experiment than that found using the LDA. Furthermore, the calculated structural properties are in excellent agreement with experiment.

ACKNOWLEDGMENTS

Helpful discussions with Dr. C. S. Wang on the numerical evaluation of V_{xc} are gratefully acknowledged. This work is supported by the National Science Foundation (NSF) under Grant No. DMR-8319024, and by a program development fund from the Director of the Lawrence Berkeley Laboratory. One of us (M.S.H.) acknowledges support from the IBM Corporation.

[1]P. Hohenberg and W. Kohn, Phys. Rev. **136**, B864 (1964).
[2]W. Kohn and L. J. Sham, Phys. Rev. **140**, A1133 (1965).
[3]E. Wigner, Phys. Rev. **46**, 1002 (1934); L. Hedin and B. I. Lundqvist, J. Phys. C **4**, 2064 (1971).
[4]U. von Barth and L. Hedin, J. Phys. C **5**, 1629 (1972); O. Gunnarsson, B. I. Lundqvist, and J. W. Wilkens, Phys. Rev. B **10**, 1319 (1974).
[5]D. M. Ceperley, Phys. Rev. B **18**, 3126 (1978); D. M. Ceperley and B. I. Alder, Phys. Rev. Lett. **45**, 566 (1980). These results are parametrized in J. P. Perdew and A. Zunger, Phys. Rev. B **23**, 5048 (1981).
[6]For metallic systems, refer, for example, to V. L. Moruzzi, J. F. Janak, and A. R. Williams, *Calculated Properties of Metals* (Pergamon, New York, 1978); M. Y. Chou, P. K. Lam, and M. L. Cohen, Phys. Rev. B **28**, 4179 (1983); P. K. Lam and M. L. Cohen, *ibid.* **24**, 4224 (1981); S. G. Louie, F. Froyen, and M. L. Cohen, *ibid.* **26**, 1738 (1982).
[7]For semiconductors, refer, for example, to J. Ihm and J. D. Joannopoulos, Phys. Rev. B **24**, 4191 (1981); M. T. Yin and M. L. Cohen, *ibid.* **26**, 5668 (1982); S. Froyen and M. L. Cohen, Solid State Commun. **43**, 447 (1982).
[8]D. R. Hamann, Phys. Rev. Lett. **42**, 662 (1979).
[9]For the case of wide-gap insulators, see, for example, R. A. Heaton and C. C. Lin, Phys. Rev. B **22**, 3629 (1980); S. B. Trickey, F. R. Green, Jr., and F. W. Averill, *ibid.* **8**, 4822 (1973).
[10]G. Strinati, H. J. Mattausch, and W. Hanke, Phys. Rev. B **25**, 2867 (1982), and references therein.
[11]C. S. Wang and W. E. Pickett, Phys. Rev. Lett. **51**, 597 (1983).
[12]L. J. Sham and W. Kohn, Phys. Rev. **145**, 561 (1966).
[13]L. Hedin, Phys. Rev. **139**, A796 (1965).
[14]Z. H. Levine and S. G. Louie, Phys. Rev. B **25**, 6310 (1982).
[15]K. S. Singwi, M. P. Tosi, R. H. Land, and A. Sjölander, Phys. Rev. **176**, 589 (1968); K. S. Singwi, A. Sjölander, M. P. Tosi, and R. H. Land, *ibid.* B **1**, 1044 (1970).
[16]A. Zunger, J. P. Perdew, and G. L. Oliver, Solid State Commun. **34**, 933 (1980); J. P. Perdew and A. Zunger, in Ref. 5.
[17]R. A. Heaton, J. G. Harrison, and C. C. Lin, Solid State Commun. **41**, 827 (1982).
[18]J. P. Perdew and M. R. Norman, Phys. Rev. B **26**, 5445 (1982).
[19]L. J. Sham and M. Schlüter, Phys. Rev. Lett. **51**, 1888 (1983).
[20]J. P. Perdew and M. Levy, Phys. Rev. Lett. **51**, 1884 (1983).
[21]D. C. Langreth and M. J. Mehl, Phys. Rev. B **28**, 1809 (1983), and references therein.
[22]J. A. Alonso and L. A. Girifalco, Solid State Commun. **24**, 135 (1977); J. A. Alonso and L. A. Girifalco, Phys. Rev. B **17**, 3735 (1978).
[23]O. Gunnarsson, M. Jonson, and B. I. Lundqvist, Solid State Commun. **24**, 765 (1977); Phys. Rev. B **20**, 3136 (1979).
[24]F. Manghi, G. Rieglar, C. M. Bertoni, C. Calandra, and G. B. Bachelet, Phys. Rev. B **28**, 6157 (1983); Phys. Rev. B **29**, 5966(E) (1984).
[25]M. S. Hybertsen and S. G. Louie, Solid State Commun. **51**, 451 (1984).
[26]O. Gunnarsson and B. I. Lundqvist, Phys. Rev. B **13**, 4274 (1976).
[27]O. Gunnarsson and R. O. Jones, Phys. Scr. **21**, 394 (1980).
[28]J. Callaway, Phys. Rev. **116**, 1368 (1959).
[29]G. P. Kerker, Phys. Rev. B **24**, 3468 (1981).
[30]G. Borstel, M. Neumann, and W. Braun, Phys. Rev. B **23**, 3113 (1981).
[31]H. Przybylski and G. Borstel, Solid State Commun. **49**, 317 (1984).
[32]G. P. Kerker, J. Phys. C **13**, L189 (1980).
[33]J. Ihm, A. Zunger, and M. L. Cohen, J. Phys. C **12**, 4409 (1979).
[34]D. J. Chadi and M. L. Cohen, Phys. Rev. B **8**, 5747 (1973).
[35]*Landolt-Börnstein: Zahlenwerte und Funktionen aus Naturwissenschaften und Technik* (Springer, New York, 1982), Vol. III, pt. 17a.
[36]W. E. Spicer and R. C. Eden, in *Proceedings of the Ninth International Conference of the Physics of Semiconductors, Moscow, 1968* (Nauka, Leningrad, USSR, 1968), Vol. 1, p. 61.
[37]R. Hulthen and N. G. Nilsson, Solid State Commun. **18**, 1341 (1976).
[38]This appears to contradict the results of Manghi *et al.* in Ref. 24. However, there is an error in their WDA calculation as reported in their erratum, and the new results agree with our observation of improved band gaps.
[39]F. D. Murnaghan, Proc. Nat. Acad. Sci. U.S.A. **30**, 244 (1944).
[40]J. Donohue, *The Structure of the Elements* (Wiley, New York, 1974), extrapolated to 0 K.
[41]L. Brewer, Lawrence Berkeley Laboratory Report No. LBL-3720 (unpublished), May 1977 revision.
[42]P. J. E. Aldred and M. Hart, Proc. R. Soc. London, Ser. A **332**, 223 (1973).
[43]J. B. Roberto, B. W. Batterman, and D. T. Keating, Phys. Rev. B **9**, 2590 (1974), for the (222) reflection in Si.
[44]T. Matsushita and K. Kohra, Phys. Status Solidi A **24**, 531 (1974).
[45]S. B. Trickey, A. K. Ray, and J. P. Worth, Phys. Status Solidi B **106**, 613 (1981).